

# Addressing memory bandwidth scalability in vector processors for streaming applications

JORDI ALTAYÓ, PAUL DELESTRAC, and AHMED HEMANI, KTH - Royal Institute of Technology, Sweden  
 DAVID NOVO, LIRMM - Laboratoire d'informatique, de robotique et de microélectronique de Montpellier, France  
 SIMEY YANG\*, South China University of Technology, China  
 DEBJYOTI BHATTACHARJEE and FRANCKY CATHOOR, IMEC - Interuniversity Microelectronics Centre, Belgium

As the size of artificial intelligence and machine learning (AI/ML) models and datasets grows, the memory bandwidth becomes a critical bottleneck. The paper presents a novel extended memory hierarchy that addresses some major memory bandwidth challenges in data-parallel AI/ML applications. While data-parallel architectures like GPUs and neural network accelerators have improved power performance compared to traditional CPUs, they can still be significantly bottlenecked by their memory bandwidth, especially when the data reuse in the loop kernels is limited. Systolic arrays (SAs) and GPUs attempt to mitigate the memory bandwidth bottleneck but can still become memory bandwidth throttled when the amount of data reuse is not sufficient to confine data access mostly to the local memories near to the processing. To mitigate this, the proposed architecture introduces three levels of on-chip memory — local, intermediate, and global — with an ultra-wide register and data-shufflers to improve versatility and adaptivity to varying data-parallel applications. The paper explains the innovations at a conceptual level and presents a detailed description of the architecture innovations. We also map a representative data-parallel application, like a convolutional neural network (CNN), to the proposed architecture and quantify the benefits vis-a-vis GPUs and representative accelerators based on systolic arrays and vector processors.

CCS Concepts: • **Hardware** → **Application specific instruction set processors**.

Additional Key Words and Phrases: ASIP, DSIP, Machine Learning, Accelerator, ASIC

## ACM Reference Format:

Jordi Altayó, Paul Delestrac, Ahmed Hemani, David Novo, Simey Yang, Debjyoti Bhattacharjee, and Francky Cathoor. 2025. Addressing memory bandwidth scalability in vector processors for streaming applications. 1, 1 (May 2025), 23 pages. <https://doi.org/XXXXXXX.XXXXXXX>

## 1 INTRODUCTION

The *von Neumann* bottleneck [1] has been a long-standing challenge in computer architecture. The separation between memory and computation has lead to the current memory-dominated architectures, where data movement has become the main bottleneck [2, 16], both for performance and energy consumption. This effect is significantly pronounced in

\*The work was done while the author was affiliated with IMEC.

Authors' addresses: Jordi Altayó, [jordiag@kth.se](mailto:jordiag@kth.se); Paul Delestrac, [pauldel@kth.se](mailto:pauldel@kth.se); Ahmed Hemani, [hemani@kth.se](mailto:hemani@kth.se), KTH - Royal Institute of Technology, Stockholm, Sweden; David Novo, [david.novo@cnrs.fr](mailto:david.novo@cnrs.fr), LIRMM - Laboratoire d'informatique, de robotique et de microélectronique de Montpellier, Montpellier, France; Simey Yang, [simey.yang@imec.be](mailto:simey.yang@imec.be), South China University of Technology, Guangzhou, China; Debjyoti Bhattacharjee, [debjoti.bhattacharjee@imec.be](mailto:debjoti.bhattacharjee@imec.be); Francky Cathoor, [francky.cathoor@imec.be](mailto:francky.cathoor@imec.be), IMEC - Interuniversity Microelectronics Centre, Louven, Belgium.

Permission to make digital or hard copies of all or part of this work for personal or classroom use is granted without fee provided that copies are not made or distributed for profit or commercial advantage and that copies bear this notice and the full citation on the first page. Copyrights for components of this work owned by others than the author(s) must be honored. Abstracting with credit is permitted. To copy otherwise, or republish, to post on servers or to redistribute to lists, requires prior specific permission and/or a fee. Request permissions from [permissions@acm.org](mailto:permissions@acm.org).

© 2025 Copyright held by the owner/author(s). Publication rights licensed to ACM.

Manuscript submitted to ACM

data-parallel applications, such as artificial intelligence and machine learning (AI/ML), where the size of the models and datasets used in these applications has been growing exponentially [2, 3, 17, 23, 24]. When memory bandwidth becomes the bottleneck, the performance gains achieved by exploiting the data-level parallelism in these applications are overshadowed by memory accesses, leading to stalled processing elements and wasted energy [5, 6].

An ample number of architectures have been proposed as potential solutions to the memory bandwidth bottleneck. Among these, systolic arrays (SAs), single-instruction multiple-data (SIMD), single-instruction multiple-thread (SMT), and vector processors have been the most prominent. Different flavours of them have shown potential strengths in these applications. Eyeriss [7] and TPU [4] are representative examples of SA-based, while ARA [21] and Nvidia’s Ampere GPU architecture [19] represent vector and SMT architectures, respectively.

We show how heavy reliance on data reuse can lead to memory throttling when the available level of reuse becomes insufficient to feed the memory hierarchy and to keep the data access mostly to the local memories near the processing [9, 10]. We also show how the scalability of these architectures is limited by different factors, such as the 2D organization of the PEs in SAs, or the lack of flexibility in the interconnect of the current vector processors.

We propose a vector architecture extension that addresses these limitations by introducing a novel extended memory hierarchy with scalable bandwidth, and does not rely mainly on data reuse for achieving high performance. So, it also performs well when data reuse factors are quite low, albeit at the expense of initiating more costly data move operations in that case. The architecture is based on a 1D organization of the PEs but introduces extra elements in the memory hierarchy that allow it to maintain the scalability of vector processors while maintaining the efficiency on data movement of systolic arrays. In particular, it introduces an ultra-wide single-port register and a specialized wide data shuffler.

## 1.1 Scope

This work focuses on the architectural aspects and how the memory bandwidth limitations are addressed. We do not delve into the details of the implementation of the processing elements beyond the details required to understand the data movement within them. Furthermore, to maintain the length of the paper within the limits and to conceptually split the work between bandwidth and energy efficiency, we do not perform a detailed analysis and comparison of the energy efficiency. However, we still provide a qualitative explanation on why the proposed memory hierarchy is, at least, as energy efficient as an equivalently sized alternative, with potential for obtaining significant gains when scaling the architecture. We leave a detailed analysis of the energy efficiency for future work.

## 1.2 Contributions and paper organisation

The contributions of this work are organized as follows:

- We identify the limitations of the current architectures based on GPUs, systolic arrays and vector processors, and motivate the need for the addition of the architectural elements proposed in this work in Section 3.
- We propose an architecture extension that addresses these limitations by introducing a modified memory hierarchy that is scalable and does not rely mainly on data reuse for achieving high performance. So, it even functions under low data reuse factors. We also include the processing elements emphasizing the data shufflers in Section 4.
- We present a detailed comparison at the architectural level with the four architectures mentioned above: Eyeriss, TPU, ARA, and GPUs in Section 5.

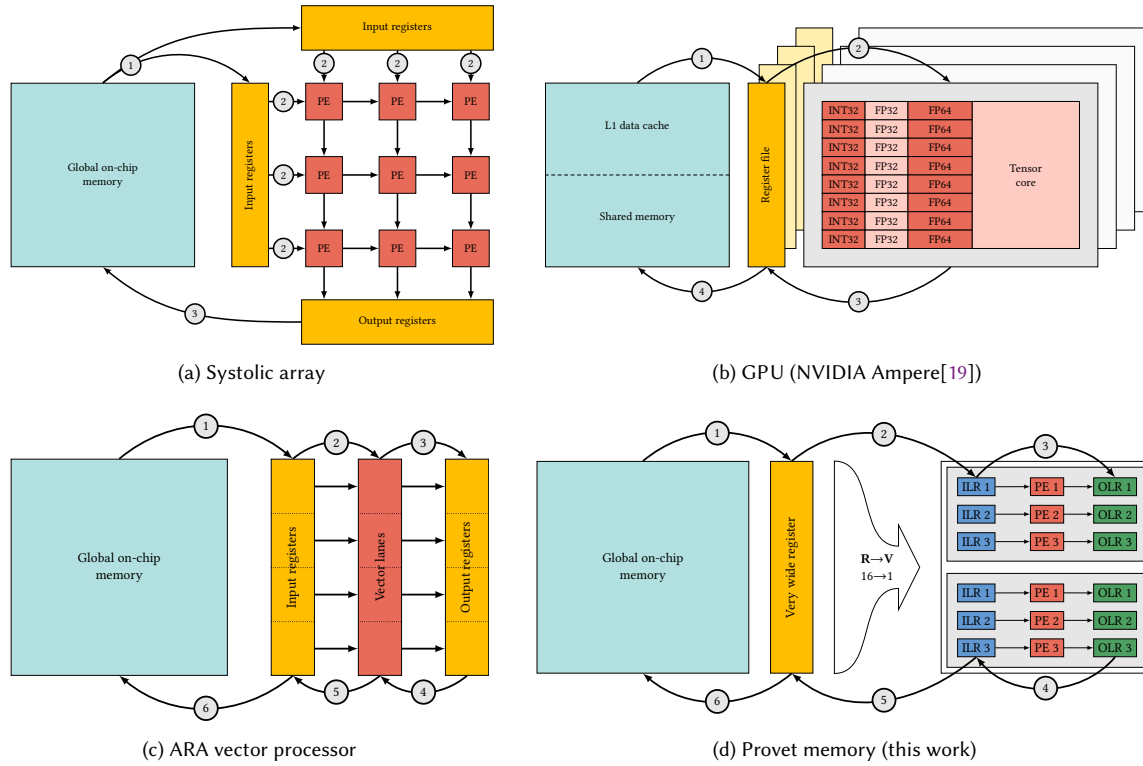


Fig. 1. Comparison of the memory hierarchies. The numbered white arrows show the possible paths data can take in the architecture when moving up and down the memory hierarchy through the processing elements (PEs)

- We show how a representative data-parallel application is mapped to the proposed architecture in Section 6, emphasizing the usage of the architectural extensions proposed in this work. We also show how the convolutional kernels are combined to implement a full neural network and how size mismatches can be handled without significant overhead.
- Section 7 presents an analysis of the gains obtained by our innovations compared to the mentioned baseline architectures. This is performed for the metrics relevant to memory bandwidth (which is our main focus in this paper) such as memory accesses, latency, PE utilization, among others.

## 2 BACKGROUND AND STATE-OF-THE-ART SUMMARY

This section describes the state-of-the-art architectures that have become prominent actors in the ML/AI domain: systolic arrays, vector processors and GPUs. We primarily focus on their memory hierarchies and data movement. The next section will describe the limitations of these architectures and motivate the introduction of a new memory hierarchy to overcome some of these limitations.

Figure 1 illustrates the memory hierarchies for (1a) systolic arrays, (1c) a general vector processor (ARA [21]), (1b) a GPGPU (NVIDIA Ampere [19]), and (1d) our proposed solution, which we refer to as *Provet* hereafter. We compare these three architecture classes according to: (1) how the Processing Elements (PEs) are organized, (2) their memory hierarchy,

and (3) their interconnect. The descriptions of systolic arrays draw on MIT’s Eyeriss [?] and Google’s TPU [15], those of vector processors on PULP’s ARA [21], and those of GPUs on NVIDIA Ampere [19].

## 2.1 Systolic arrays

Systolic arrays arrange PEs in a 2D grid. Their memory hierarchy is typically straightforward, consisting of an input and an output register that supply data to, and collect results from, the array. The bandwidth between these registers and the array is limited by the number of PEs situated on the array’s boundary, which scales proportionally to the square root of the total number of PEs. The interconnect usually employs nearest-neighbor links, which simplifies hardware costs but constrains the range of possible data transfers inside the array.

Because of this layout, the organization of PEs restricts the scalability of the memory bandwidth (Section 3.1) and makes the array susceptible to mismatches in size (Section 3.2). Finally, limitations in the interconnect further constrain the kinds of dataflows that can be efficiently mapped onto the array (Section 3.3).

## 2.2 Vector processors

Conventional vector processors place PEs in a one-dimensional arrangement, with each PE connected to its own local memory (input and output registers). Data movement within a single vector lane is confined to the slice of memory allocated to that lane. Their memory hierarchy is much like that of systolic arrays, featuring an input and an output register to feed data to the array and store outcomes. However, the interconnect within a vector lane is more adaptable, allowing shuffling or permutation among PEs. On the other hand, inter-lane communication can only happen through a shared global interconnect.

Vector processors also experience issues stemming from size mismatches (Section 3.2) and are subject to interconnect limitations (Section 3.3).

## 2.3 GPUs

GPUs organize their PEs in multiple Streaming Multiprocessors (SMs) (4 PEs per SM in NVIDIA’s Ampere architecture [19]). Each PE has its own register file, and PEs within the same SM can access a shared L1 cache and/or a scratchpad (i.e., shared memory). Multiple SMs share a large L2 cache. Accessing data across SMs require traversing the higher latency L2 cache and/or main memory (i.e., HBM memory in Ampere). The memory hierarchy of GPUs is deep, with multiple levels of caches and scratchpads to enable both fast access to small caches and huge storage capacity for the big workloads of modern applications. The interconnect is more flexible than systolic arrays and vector processors, with multiple levels of caches and scratchpads that allow for more complex data movement patterns. However, the interconnect is still limited to the PEs within the same SM, and accessing data across SMs requires traversing the higher-latency L2 cache and/or main memory.

Similar to vector processors, GPUs are also sensitive to size mismatches, described in Section 3.2, and the interconnect limitations, described in Section 3.3.

## 3 MOTIVATIONS

Based on the state-of-the-art architectures described in the previous section, we identify four key limitations that motivate the introduction of a new memory hierarchy. The first two primarily affect systolic arrays, while the latter are common to both systolic arrays, GPUs and vector processors.

### 3.1 Memory bandwidth scalability

Array (2D) organizations intrinsically limit the scalability of the architecture in terms of memory bandwidth. The input and output bandwidth of the array scales with the square root of the number of processing elements, which means that the size of the array required to achieve a given bandwidth grows quadratically. This, coupled with the size mismatch (sec. 3.2) and the interconnect limitations (sec. 3.3) limits the size of the array that can be used in practice. Thus, the memory bottleneck can only be mitigated by exploiting the data reuse within the array, which is not always possible in all applications. We show in section 7 how some networks which exhibit little data reuse, like MobileNet or SqueezeNet, lead to a significant underutilization in array-based architectures (e.g., Eyeriss, TPU).

This limitation is addressed in section 5.1.

### 3.2 Size mismatch sensitivity

Increasing the size of the arrays to achieve higher memory bandwidth can result in arrays that are too large to naturally fit the dimensions of the application kernels. Complex dataflows and folding methods are required to map the application to the array to fully utilize the array. Even when using automatic dataflow design-space exploration tools [18, 20], the rigid interconnect of the array can limit the options and force the data to jump over multiple PEs, which increases the overhead and latency. This issue is further exacerbated with the scaling of the array size. Linear (1D) organization of the processing elements can mitigate this problem as data can be linearly spatially distributed in the memory, which allows for a direct path between memory and PEs, removing the jumps and not limiting the scalability of the array. The key difference between linear (1D) vs array (2D) organizations is that data can only be fed to the edge PEs of the arrays, while linear organizations can deliver data to all the PEs. Refer to Figure 1.

This limitation is addressed in section 5.2.

### 3.3 Interconnect limitations

Interconnects in both systolic arrays, vector processors and GPUs are simple and rigid. This is a conscious design choice to minimize the overhead and complexity; however, it can limit the flexibility and restrict the operations that can be naturally mapped to the array. For the relevant case of convolutional kernels, the sliding nature of the kernel cannot be naturally mapped without having to use im2col transformations or its derivatives. Such transformations are required to exploit the efficient GEneral Matrix Multiplication (GEMM) kernels present in commonly used linear algebra libraries, such as NVIDIA cuBLAS [8]. However, im2col introduces large data redundancy. For example, a  $7 \times 7$  kernel with a stride of 1 convolving a  $256 \times 256$  image requires a  $7^2 \times 256^2$  matrix, going from 65 thousand elements to 3 million elements, a  $\times 46$  increase. Furthermore, the large size difference between the matrices can lead to performance decreases [12, 25] and the overhead of the transformation can be significant for small kernels. Even when using more efficient variations of the im2col transformation, such as implicit GEMM, can lower the memory overhead by one order of magnitude, the overhead will always be higher than a factor of two (100%) [26].

This limitation is addressed in section 4.2, where we show how a more flexible interconnect can allow for more complex data movement patterns that support the sliding nature of the convolutional kernel.

### 3.4 Dependency on data reuse

Systolic arrays, vector processors and GPUs rely heavily on data reuse to reduce the memory accesses and maintain a high utilization of the processing elements. However, not all ML and AI workloads exhibit high data reuse, which

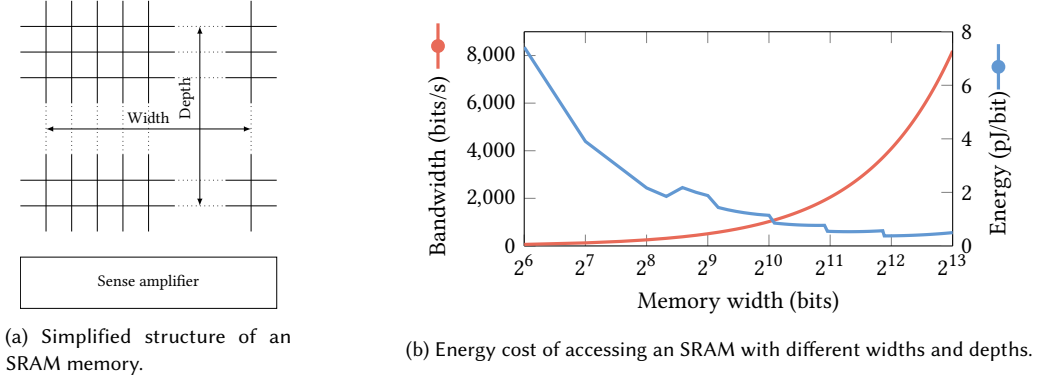


Fig. 2. Simplified SRAM memory structure and energy cost estimations.

could lead to underutilization of the array and suboptimal performance. A common example in CNN are depth-wise separable convolutions, found in the MobileNet class CNNs [13].

We show in section 7 how our proposal does not rely on data reuse to mitigate the memory bottleneck challenges, although data reuse greatly benefits that aspect, even in applications with little data reuse, the design is not memory-throttled. Any additional data reuse will enhance the performance and reduce the memory accesses on top of the obtained by the architectural gains.

#### 4 DETAILED ARCHITECTURAL DESCRIPTION

In this section, we present a vector architectural template that mitigates the limitations of current architectures based on systolic (2D) and vector (1D) arrays. The proposed architecture, hereafter referred to as Provet, is based on a 1D organization, however it introduces extra elements in the memory hierarchy and interconnect making it significantly different from traditional vector processors or GPUs. This section describes Provet's architecture in detail, including the memory hierarchy, components, and control structure. The next section (sec. 5) compares the proposed architecture with others, highlighting key differences. While it borrows many concepts, such as the linear (1D) organization, the added elements introduce significant improvements and distinctions which we detail in this section.

##### 4.1 Memory hierarchy

We propose an ultra-wide and shallow memory as the main global on-chip memory. An ultra-wide memory inherently has a very high bandwidth, while maintaining a low energy consumption. This can be understood by observing that the energy cost of accessing an SRAM consists of two main components: width-dependent and depth-dependent. The analysis is targeted to Provet SRAM memory because this paper focuses only on on-chip aspects of the architecture. Although the same conclusions can be drawn for off-chip memories, the analysis for the implications on the interconnect of off-chip memories falls out of the scope of this paper.

As illustrated in Figure 2a, the length of the word lines is proportional to the number of bit lines  $W$ , while the length of the bit lines is proportional to the depth of the memory  $D$ , representing the number of word lines. Let the energy cost per unit length of the bit and word lines be denoted as  $BL$  and  $WL$ , respectively. Consequently, the cost of energizing a single bit line and word line would  $D \cdot BL$  and  $W \cdot WL$  respectively. To access one word requires energizing all  $W$  bit

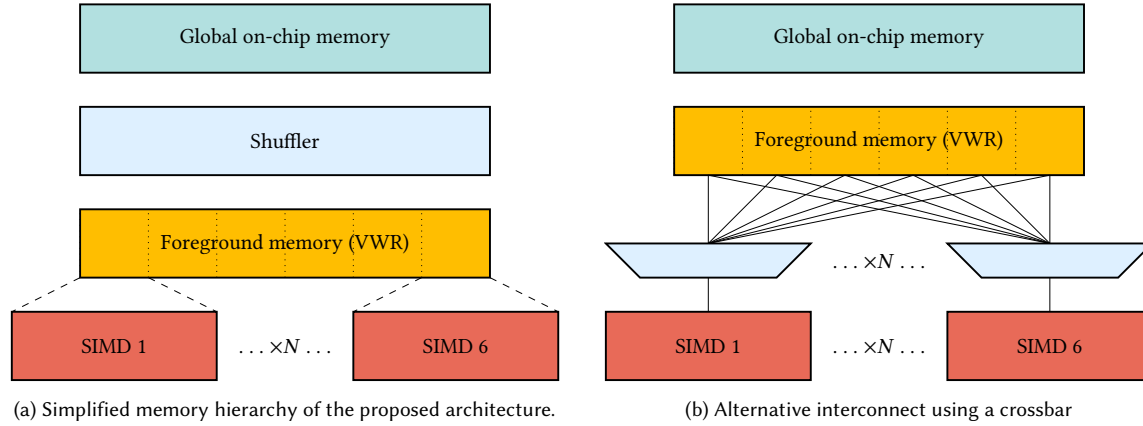


Fig. 3. Memory hierarchy and interconnect of two implementation variants of the proposed architecture.

lines, and one word line as expressed below:

$$\underbrace{W \cdot D \cdot BL}_{\text{energize } W \text{ bitlines}} + \underbrace{1 \cdot W \cdot WL}_{\text{energize 1 wordline}} \quad (1)$$

To gauge the impact of the width of memory on accessing a single word, we normalize the above expression with the width as shown below.

$$\frac{W \cdot D \cdot BL + 1 \cdot W \cdot WL}{W} = D \cdot BL + WL \quad (2)$$

This shows that maintaining an ultra-wide and shallow memory provides a high bandwidth while maintaining a low access cost, compared to an equivalent memory with a less aggressive aspect ratio.

To validate such claims, we have performed a simple simulation of the energy cost of accessing an SRAM with different widths and depths using the CACTI tool [14] and present the results in Figure 2b. It is clear that the energy cost per bit decreases with the width of the SRAM, while the bandwidth increases. This validates the lack of an energy consumption penalty when using an ultra-wide memory.

While the ultra-wide memory provides a low energy access cost, accessing it repeatedly for each computation would still cause a significant energy overhead. To mitigate this, we introduce a foreground memory (see Fig. 3a) in the form of a very wide register (VWR) that acts as a buffer between the ultra-wide memory and the vector SIMD units. This register is a single (ultra-wide) word register and *not* a multi-port register file. This means that it does not have an address space thus it does not have the overhead of the address decoding and the multiplexing of the data (which happens in a multi-port register file). Furthermore, the VWR has an asymmetric interface that matches the width of the ultra-wide memory and the SIMD units, on the other hand, as shown in Figure 3a. The asymmetry in the VWR provides an alternative mechanism to reduce the amount of memory accesses on top of the inherent data reuse in the application. In a general case, the number of accesses to the VWR will be  $N$  times higher than the number of accesses to the SRAM memory, where  $N$  is the width ratio between the SRAM width and the SIMD width. Any data reuse present in the application will further reduce the number of accesses to the SRAM memory. The experiment results

Table 1. Comparison of the area of the proposed shuffler and a generic crossbar implementation.

	Shuffler	Crossbar	Difference
<b>Area</b> (mm <sup>2</sup> )	0.13	0.88	×6.82
<b>Gate count</b>	16k	86k	×5.38
<b>Wire length</b> (mm)	4.3	33.1	×7.67

presented in section 7 validate this claim by showing a significant improvement in the compute-to-memory access ration in situations where other architectures heavily throttle due to limited data reuse.

## 4.2 Interconnect

The interconnect between the VWR and SIMD units is pitch-aligned to simplify the layout and create a regular structure. This means that each SIMD unit can access only a specific slice of the VWR. To allow SIMD units to access data that is not aligned with their slice, we introduce a shuffler. This shuffler is positioned between the SRAM and the VWR and it can be customized to provide different shuffling patterns, granularities, and ranges. The shuffling operations required are determined by profiling the application or application domain.

This interconnect choice is a conscious design decision to minimize the overhead and complexity that could result in a severe area and energy penalty. Even though the energy analysis is not the focus of this work, we have performed a simple comparison of the post-layout area of the proposed shuffler and a generic crossbar implementation (see Fig. 3b) and present the results in Table 1. The results show that the shuffler has a significantly smaller footprint in terms of area, gate count and wire length. However, we show in section 6.1 that the simple shuffler can still provide the necessary flexibility to implement complete CNN layers without any performance penalty.

The connections inside the SIMD units are a bit more flexible. We introduce multiplexers that allow the data to be moved between the VFU (vector arithmetic unit) and the local registers. This allows the local registers to be used as temporary storage for operations like accumulation. The specific details of the individual components of the architecture are presented in the next section.

## 4.3 Detailed architecture description

A detailed diagram of the architecture can be seen in Figure 4. We now present the elements seen in the figure.

**4.3.1 Ultra-wide shallow SRAM memory.** the bulk of the data that will be fetched in the short-term future by the computation elements. To leverage the properties explained in 4.1 the width of the SRAM is 8× bigger than the size of the SIMD unit, however, the depth of the SRAM is small, in the order of 1–32 words.

**4.3.2 Wide coarse-grained tile shuffler.** is located in between the SRAM and the VWRs. The shuffler implements the data rearrangement concept explained in ???. The tile shuffler is responsible for the coarse shuffling operations, i.e. it moves large blocks of data but the granularity of the shuffling distances is coarse. For example, the tile shuffler operates in blocks of data with the same size as the VWR blocks (for eg. 512 bits) and it moves the block in steps of this same size (also 512 bits). The shuffler can be customized with different shuffling capabilities, depending on the application needs.

**4.3.3 Narrow fine-grained VFU shuffler.** is located between the VWR and the SIMD units. The shuffler is responsible for the fine shuffling operations, i.e. it moves small blocks of data within a SIMD word. There are two dimensions of the



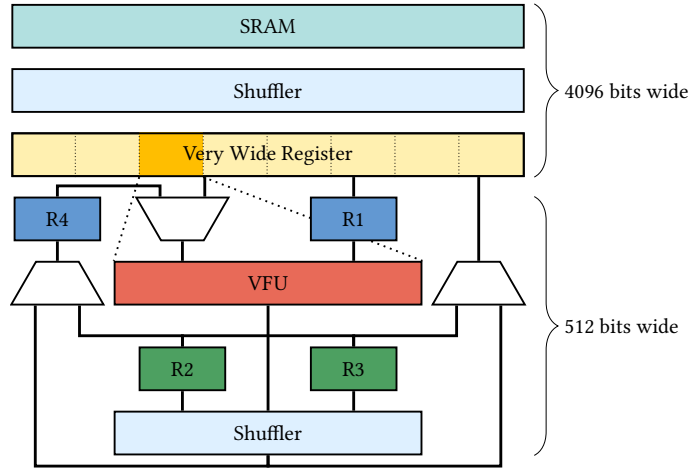


Fig. 4. Proposed architecture overview. The ultra-wide elements (4096 bits) and the SIMD unit (512 bits) are not drawn to scale to simplify the diagram.

shuffler. One is the size of the blocks it moves or shuffles. As stated above, this is decided by the aggregate width of VFU ports. The other dimension is the maximum range in terms of steps; each step is equal to the size of the blocks. A large max range will make the shuffler expensive and inefficient. This dimension is decided by profiling the intended application or application suite to find out the most widely used range of steps. Note that it is possible to go beyond the max range by using multiple steps, at the cost of more cycles.

**4.3.4 Very Wide Register (VWR).** is an single-row memory buffer placed between the SRAM and the VFUs. Usually 2 VWRs are allocated to enable concurrent reads and writes to each of these. But even solutions with a single VWR can function well on condition that the mapping is carefully optimized to accommodate this restriction. The VWR takes to the extreme the concept explained in ???. The depth of the VWR is 1, and the width is matched to the SRAM width. The VWR also has asymmetric port sizes that match the widths of the SRAM and the VFUs. The ratio between the VWR ports translated into at least a similar ratio of memory accesses. In practice, thanks to the typically big data reuse opportunities in machine learning computations the memory access ratios are much bigger. This is exemplified in section 6.1 with an illustrative example of a CONV layer. Still, as already mentioned some ML topologies don't exhibit this large data reuse and they are the most suited candidates for mapping to Provet.

The VWRs are meant to be pitch aligned with the VFUs for a simpler layout, which implies that only the VFU that physically aligns with a portion of data in the VWR can access it. The tile shuffler (sec. ???) is used to allow VFUs to access data that is not specifically aligned to them. Given the simplified interconnection between the VWRs and DPUs, the cost of accessing the VWR data is significantly lower than SRAM. The VWRs are used to store the data used in the inner loops of the application. For each transaction between the VWR and the SRAM, the VWR will serve data to the DPUs for several cycles. Ideally, this ratio should match the ratio between the VWR port sizes. However, due to limitations for the data arrangement, it will typically be lower. If the subwords in that data need to be rearranged during the loop iteration, the DPU shifter can be used (4.3.7).

**4.3.5 Local registers.** In the proposed architecture, there are four local registers: R1 to R4, as shown in Figure 4. These registers are typically used to store the weights of the filter in a weight-stationary dataflow or the partial sum in an output-stationary dataflow. The size of the registers matches the width of the VFU.

**4.3.6 Vector Functional Unit (VFU).** is an SIMD (Single Instruction Multiple Data) computation unit. The number of parallel lanes is parametric but natural values are in the 16–64 range. The width of each operand is typically 8 bits, resulting in a total width of 128–512 bits. The VFU implements the basic operations needed for ML workflows, such as addition, multiplication, non-linear functions (tanh, sigmoid). A complete list of the VFU modes can be seen in Table 2.

All VFU computations take 2 operands as inputs and produce an output (with the exception of the non-linear functions). One of the inputs of the VFU will come from R1 and the other from either R4 or VWR. The output of the VFU can be: stored in R2 or R3, sent to R4 or VWR (or both), or sent through the VFU shuffler.

The number of VFUs is parametric and can range from 1 to the width of the SRAM. Increasing the number of VFUs enhances the parallel capabilities of the architecture. Different VFUs can execute different instructions simultaneously.

**4.3.7 VFU shuffler.** complements the tile shuffler by providing fine shuffling granularity but small ranges. The shuffling range of the VFU shuffler is at most the width of the VFU and the granularity is the size of one operand. This shuffler is key to implementing operations that include a “sliding” of data, such as CONV, MAXPOOL, and AVGPOOL layers, among others.

The shuffler operates from the output of the VFU or R2/R3 registers. Additionally, it can operate directly from the output of the VWR, bypassing the VFU. This can be useful when data needs to be rearranged inside the VWR but no computation is needed.

#### 4.4 Control structure

Even though the control structure of the architecture is not the main focus of this work, for completeness we briefly describe the instructions Table 2 and DPU modes (VFUX instruction).

Due to the very wide nature of this architecture, it can become challenging to effectively control all the resources without requiring very long control wires that would have a negative impact on the energy efficiency. To overcome that we propose to decompose each instruction into its “control actions”. For example, an instruction that adds R1+VWR and stores it into R2 needs to take the following control actions: configure the VFU mode; enable the VWR, R1 and R2; configure the multiplexers to select the appropriate inputs. Each of these control actions can be performed by a distributed control element without the need for a central control unit. We call these distributed elements *loop buffers*.

The Loop Buffers (LBs) replace the centralized controller that would typically drive the control signals for all components and instead each loop buffer controls only the component it is associated with. This greatly reduces the length of the most active control signal wires which have to be activated every cycle when that part of the VFU is operational. Due to the nature of LB, LB content updates occur much less frequently (10–100× less).

The detailed implementation of the loop buffers and overall control structure falls out of the scope of this paper. We plan to address all these aspects in future work.

### 5 CONCEPTUAL COMPARISON WITH OTHER ARCHITECTURES

The architecture introduced here diverges in several respects from two-dimensional systolic arrays and from one-dimensional GPU/vector arrays. In this section, we focus on the conceptual distinctions. These distinctions are subsequently assessed in section 7. Because Provet shares similarities with other data-parallel subword-oriented vector

Table 2. Instruction set description

Instr.	Description
<b>NOP</b>	No-operation
Data Transfer Instructions	
<b>RLB</b>	Transfers data between SRAM and VWR
<b>WLB</b>	Transfers data between VWR and SRAM
<b>VMV</b>	Transfers data between VWR and local DPU registers
Data Rearrangement Instruction	
<b>GLMV</b>	Shuffles the VWR content and store back to itself
<b>RMV</b>	Shuffles the local DPU register content and stores it to VWR
<b>PERM</b>	Permutates at word-level using the DPU shuffler using a list of (source, destination) pairs that represent the movement of the words
Computation Instruction	
<b>VFUX</b>	DPU instructions with the following modes: Multiply, add, max, multiply-accumulate, add-accumulate, max-accumulate, clip, shift, RELU, sigmoid, tanh
<b>CALC</b>	Scalar operations using local DPU registers
Control Instruction	
<b>BRAN</b>	Branch instruction

(1D) architectures, we will mainly focus our detailed comparison there. In contrast, we will limit our comparison with systolic arrays to bandwidth and scalability considerations.

Due to insufficient detailed microarchitectural data on commercial GPU internals, our comparison with GPUs will be restricted to the memory hierarchy and the interconnect.

### 5.1 Memory bandwidth and scalability

Systolic arrays typically employ SRAM widths considerably narrower than those proposed in this work. Common SRAM widths range from 128 to 512 [15]. Section 3 describes why wider SRAMs can be more energy-efficient; however, another critical distinction lies in the memory bandwidth and how it scales.

As discussed in section 3, the memory bandwidth of a systolic array is constrained by the square root of the total number of PEs (Figure 5a). This arises because the memory connects only to the edge PEs, requiring data to be propagated through the interconnect network to reach those in the interior of the array. Additionally, the utilization of these PEs depends on folding the input data across the array. As shown in Fig. 5b, acceptable PE utilization is only reached when the array is large enough to accommodate multiple folds of the input data. However, this conflicts with the earlier observation that memory bandwidth emerges as a bottleneck when the array size increases.

In contrast, the proposed architecture ensures that memory bandwidth does not limit the utilization of the PEs (VFUs) with a scaling number of PEs, as the memory bandwidth increases accordingly with the number of PEs. Owing to the very wide memory, Provet’s bandwidth scales linearly with the number of PEs, whereas in a systolic array it grows with the square root of the PEs’ count (due to their square arrangement). Because of the asymmetry in the VWR ports, each VFU needs  $N$  cycles to consume the entire VWR, where  $N$  is determined by the ratio of the SRAM’s width to the

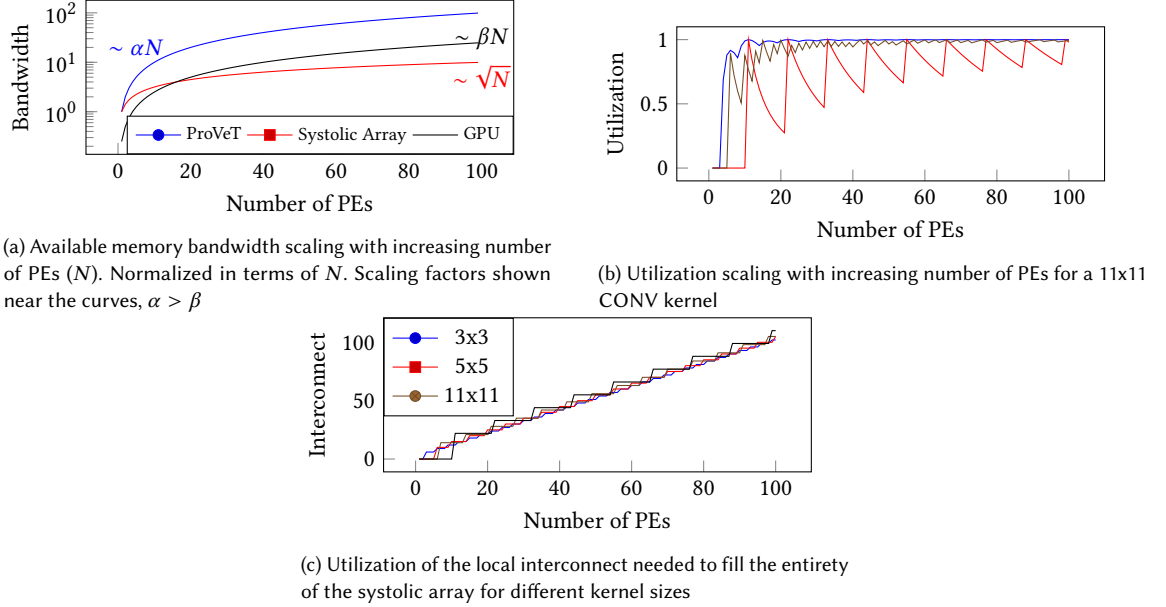


Fig. 5. Comparison between Provet and an ideal systolic array

width of the VFU. Instead, SAs rely on local data reuse to offset memory bandwidth limitations. When data reuse is limited, this constrained bandwidth can lead to under-utilized PEs. This effect is particularly evident with depth-wise separable convolutions, as will be shown in section 7.

## 5.2 Interconnect organization

A second major distinction from systolic arrays lies in how Provet manages local data movement. Systolic arrays rely on nearest-neighbor interconnects, which effectively route data in a linear sequence from one PE to the next. This approach is suitable when the dataflow can be organized so that partial sums or other intermediate values move efficiently through adjacent PEs. However, when data must traverse larger distances, the additional energy consumption and latency can become problematic. A typical scenario arises when the input image dimensions do not align with the dimensions of the SA, requiring *folding* across the 2D PE grid. In such cases, the once-linear dataflow is disrupted and data must jump across multiple PEs. The resulting increase in communication latency can lower utilization when needed data arrives too late, forcing PEs to idle.

Provet, in contrast, uses shufflers to facilitate the necessary local data transfers to the VFUs. These shufflers can link different VFU slots in a single cycle over significant distances. It is important to note that the maximum shuffler range is determined at design time and should be guided by application profiling. If a large shuffling distance is rarely used, the designer could restrict the maximum range and rely on two consecutive shuffle operations instead. Long shuffling distances can lead to an increase in wire length and thus energy consumption. For this reason, the size of the shuffler should be selecting based on a trade-off between the energy efficiency and the performance based on profiling. As shown in Section 6, a shuffle distance of 1 is sufficient to implement the CONV and fully connected kernels. It is important to note that the length of the wires will scale with the shuffle distance and not with the size width of the

shuffler (and Provet). If the shuffling distance stays the same, the length of the wires and thus (normalized) energy consumption will not increase with an increase of width.

Moreover, local data movement in Provet generally proceeds vertically: data from a specific SRAM location is mostly directed to the VFU slot that is vertically aligned, which reduces the frequency of horizontal transfers through the shufflers. This characteristic is illustrated in the CONV example (section 6.1).

Figure 5c shows that, in an SA-based approach, interconnect usage scales with the size of the array. Because data enters primarily at the array’s boundaries, more PEs entail longer paths through the network before data reaches those located centrally. By contrast, in Provet, interconnect utilization remains relatively constant since all PEs have direct access to memory through the VWR.

### 5.3 Memory hierarchy

A primary distinction between Provet and other architectures lies in its memory hierarchy. Figure 3a illustrates the various elements of that hierarchy as well as the interconnections among them.

**5.3.1 Systolic arrays.** They use a single global memory that supplies the entire array. They also incorporate input and output registers for storing stationary data (input) and partial results (output) during computation. Data movement always proceeds by (1) transferring data between the global memory and the input registers, (2) feeding data into the PE array, (3) circulating data within the array for as long as reuse opportunities remain, and (4) eventually returning data from the output registers to the global memory. As mentioned earlier, all mechanisms aimed at minimizing data access fundamentally hinge on the presence of data reuse within the array, which depends on the specific application. Thus, the memory hierarchy alone cannot ensure a fixed level of memory access reduction.

**5.3.2 ARA vector processor.** Its memory hierarchy is similar to that of Provet in that each PE is tied to a portion of the global memory, and a register is placed between the global memory and the SIMD units. However, this register is a standard vector register file rather than a VWR, and it primarily stores intermediate results between memory and SIMD operations. This difference can hinder scalability, as a conventional (non-ultra-wide) register tends to become an energy bottleneck when the number of PEs grows. The ARA interconnect also limits data movement among and within SIMD slices. While the general data path—moving data from global memory to the register file and then to the SIMD units—is consistent with Provet, the critical difference lies in the widths of each memory hierarchy element, which ultimately affects how effectively memory accesses can be reduced.

**5.3.3 GPUs.** They feature a memory hierarchy that is similar to the one of systolic arrays. The main difference is that the memory feeds into a 1D array of PEs, which means that the entire array can access the memory directly. GPUs do not feature any of the intermediate elements that Provet and ARA provide, which means that the access to the main memory will not show any reduction in terms of number of accesses. GPUs heavily rely on *batching* to reduce the number of memory accesses and to hide the latency of such accesses [10]. This batching however introduces a significant increase in the latency of the application. The data movement in GPUs is similar to the one in systolic arrays, where the data is (1) moved from the global memory (through levels of cache) to the intermediate register file, then (2) to the SIMD unit, and finally (3) back to the global memory. The only difference being the 1D organization of the PEs. However, data movement between PEs has to go through caches. For example, with the Ampere architecture: PEs within the same SM communicate through L1, and PEs from different SMs communicate through L2. The nature of the

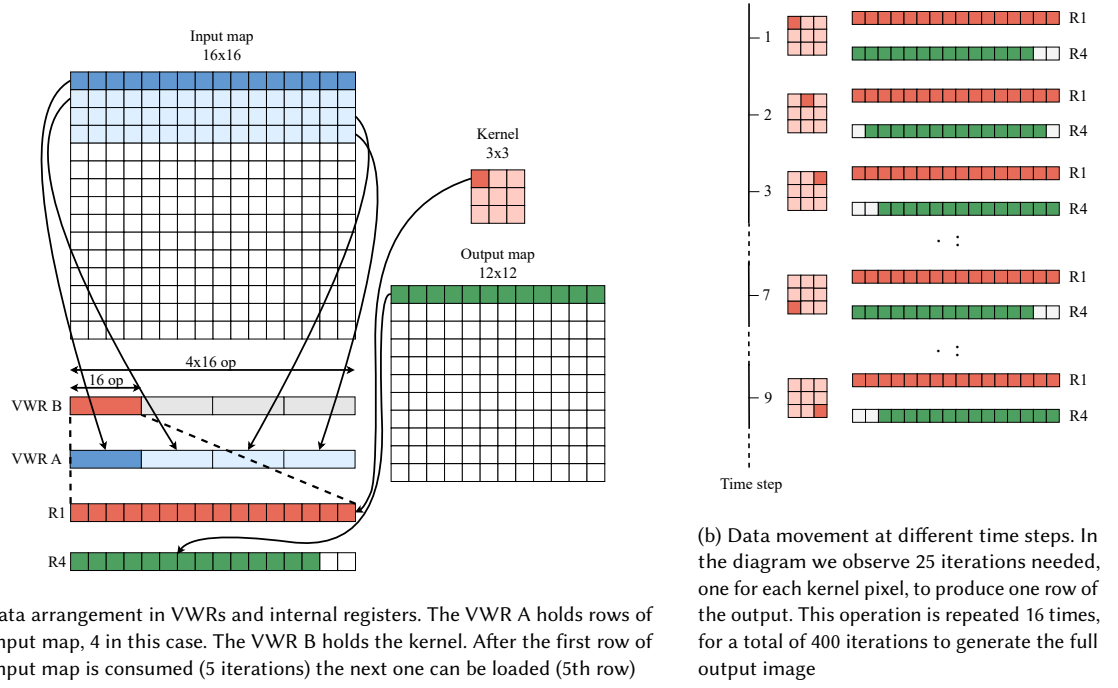


Fig. 6. Example of a convolution layer

register file in GPUs is completely different from the VWR in Provet. Regarding their sizes, the GPU register file is closer to the global memory of Provet, while conceptually closer to the VWR.

The mismatches in both functionality (asymmetry) and scale shows that the VWR has no direct equivalent element in the GPU memory hierarchy. Hence, this poses a challenge when comparing both architectures or when experimentally normalizing the sizes of memory elements for comparison. In section 7, we provide different comparisons to showcase that the improvements brought by Provet are valid in a wide range of scenarios.

## 6 MAPPING NEURAL NETWORKS

To analyze the capabilities of this architecture when executing common DNN algorithms, a set of DNN mappings has been created and analyzed. We show how two of the most common types of layers can be mapped to the proposed architecture.

### 6.1 Illustrative example of a CONV layer

In this section, we elaborate on a detailed example of a CONV layer mapping. The dimensions of both the CONV layer and architecture have been chosen small to facilitate the illustrations and provide clarity to the reader on how the data movement and organization are developed. The exact same principles that are presented in this example can be extended to real-world dimensions.

We now proceed to map a 5x5 kernel and a 16x16 input map into an architecture where 16 operands per VFU, 64 operands SRAM width, and a single VFU. Figure 6a shows how the data is arranged in the VWRs. VWR A holds the first 4 rows of the input map and VWR B holds the entire kernel.

The main idea of this dataflow is to hold the output map partial sum in R4 and iterate over all kernel pixels. In each iteration, a kernel pixel is read and broadcasted to all positions of R1. Then R1 is multiplied by an entire row of the image. Depending on which iteration, a different slice of the VWR will be selected. The result of the multiplication is accumulated into R4. Finally, R4 contents are shifted one position to the right. This process is repeated five times until the whole row of the kernel is processed. After that, R4 is shifted back to its original position, and the next row of the kernel starts.

The following pseudo-code shows the data flow presented above using the descriptive instruction names. The descriptive instruction names are used to facilitate the reading of the code and correspond to the instructions from

Table 2.

```

GLV (i, i+2N+1) # load weights
for k in range(INPUT_HGHT-KERNEL_HEIGHT-1)
  for j in range(KERNEL_HEIGHT)
    for i in range(KERNEL_WIDTH)
      read_from_vwr(VWR=B, slice=j%5, mask=i)
      vfux_mult(in1=VWRA, in2=R1, out=R2)
      vfux_add(in1=R2, in2=R4, out=R4)
      shuffle(in=R4, out=R4, step=1)
    end
    shuffle(in=R4, out=R4, step=-4)
  end
end

```

## 6.2 Dealing with size mismatches

When the size of the hardware does not match the size of the image or kernel, the mappings have to be adjusted to deal with the size mismatches. This process is typically called *folding*. In this section we show how the mapping concept presented in 6.1 can be adjusted to two different cases: image bigger than the hardware and image smaller than the hardware. Considering that the proposed architecture targets large widths (e.g. 2046 bit) the first situation will occur rarely but the second will very common.

**6.2.1 Image bigger than the width.** the solution for this situation is to partition the image into smaller parts. As shown in Figure 8, the input image can be partitioned into 4 smaller sub-images. Those sub-images can then be processed independently as a normal (smaller) image. The downside of this solution is that a portion of the image, marked in gray, will have to be duplicated. This is caused by the sliding nature of the convolution kernel. The size duplicated area is given by the size of the kernel. It is important to note that the overhead caused by this duplication will be practically negligible. As previously mentioned, the typical widths found in this architecture will be 1024-2046bit or higher. Considering that the bigger kernels that are commonly used in CNNs are 11x11, the duplicated portion of the image will be less than 5% of the total image size.

**6.2.2 Image smaller than the width.** the solution for this situation is to fit two separate images into the VWR and VFUs simultaneously. Figure 7 shows how two images and kernels are merged into the VWRs and VFUs. This particular

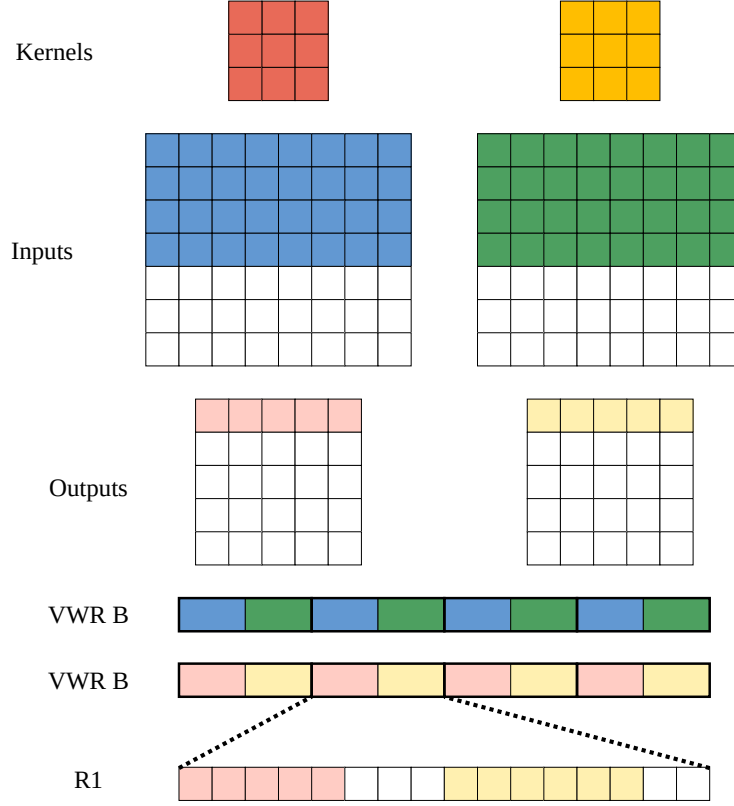


Fig. 7. Fitting 2 kernels in 1 VFU

example shows how the two images, when combined, fit exactly into the width of the VWRs. This is, however not the general case and some empty portions will often be left unfilled. These empty slots will lead to an under-utilization in the VFUs. However, it is easy to see how the utilization will asymptotically reach 100% for large widths.

### 6.3 Template system

Using the bare instructions to write complex DNN applications can be very complex and slow since it would require writing the equivalent of assembly code. We propose a template system with a basic set of templates that implement basic functions commonly used in DNNs, such as multi-dimensional convolutions, max pool, fully connected, etc. These *macros* are provided as a library that can later be used to construct more complex algorithms. The templates incorporate the two aspects of a mapping: the instructions and the memory layout. These templates aim to provide a similar interface layer that libraries such as PyTorch or TensorFlow provide for GPU architectures.

## 7 EXPERIMENTS AND RESULTS

To validate the claims put forward for the proposed architecture, we compare several mappings against two systolic array (SA) architectures—Eyeriss and TPU—alongside a vector processor (ARA) and an Nvidia Ampere GPU.



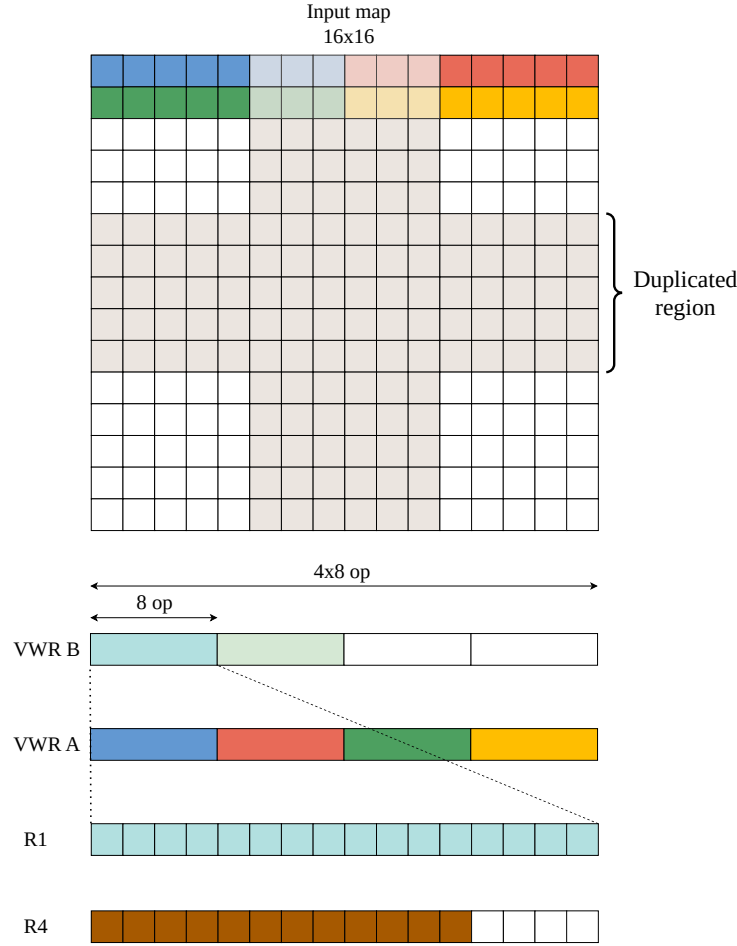


Fig. 8. Fitting 1 input map wider than the VFU

For TPU and Eyeriss, mappings are generated using the ZigZag design space exploration framework, along with the hardware and mapping templates provided for those architectures to align with their respective publications [7, 15]. The ARA mappings are derived from the code snippets provided by the original authors. GPU mappings are implemented using TensorFlow and the cuDNN library, the metrics are extracted using the methodology proposed by Delestrac et.al. [11]. The Provet mappings are produced according to the methodology introduced in section 6.

Figure 9 presents the utilization results for various layers of ResNet, AlexNet, and MobileNet. Provet's utilization figures derive from manual mappings, whereas for the ZigZag-generated mappings, utilization is computed as the ratio of the theoretical minimum latency to the observed latency, as given in equation (3). In this equation,  $L_{\min}$  is the minimum latency, and  $L_{\text{real}}$  is the actual latency of the mapping. The minimum latency is obtained by summing all MAC operations within a layer and dividing by the total number of PEs. The real workload-dependent latency is

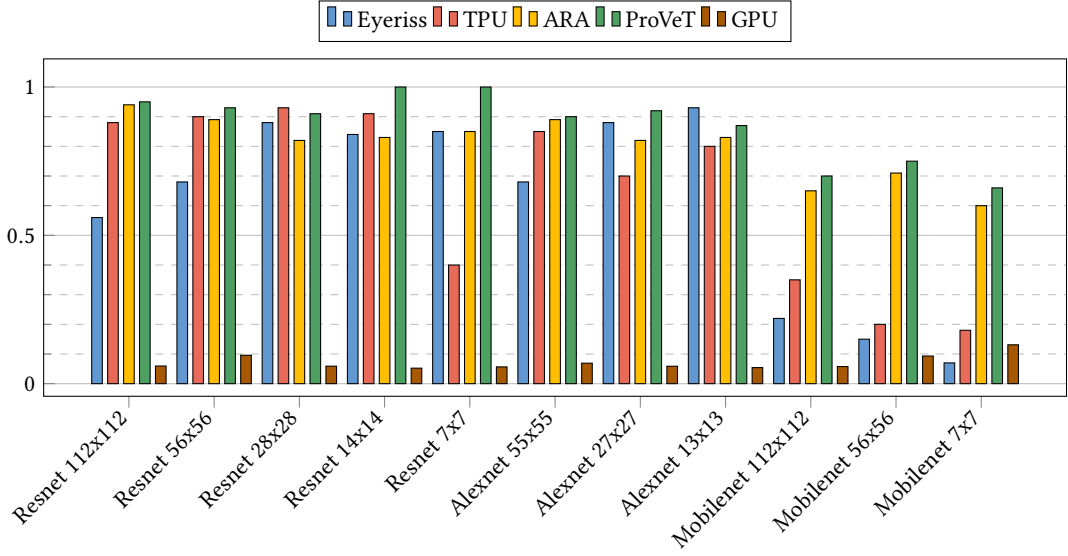


Fig. 9. PE utilization for different layers of state-of-the-art CNNs.

determined by analyzing the DSE results to count the number of cycles used to process the layer. The GPU utilization is calculated by considering only the memory-related stalls, as the other architectures do not include the control overhead in their models. This is done by collecting the amount of control stalls and their relative occurrence, which is found to be 75.6% of the total stalls (see Fig. 11b). The GPU utilization is then scaled up by this factor to provide a fair comparison with the other architectures.

The compute-to-memory instruction ratio is computed by recording the total number of compute instructions (executed in the VFU) and the total number of memory instructions (executed in the global data buffer), and then forming the quotient. Equation (4) captures this formally. A high ratio indicates that the architecture performs more computations per memory access, while a low ratio implies that the architecture is limited by memory bandwidth, as the PEs cannot remain fully occupied.

$$U = \frac{L_{\min}}{L_{\text{real}}} \quad (3)$$

$$CMR = \frac{N_{\text{compute}}}{N_{\text{memory}}} \quad (4)$$

To summarize, Table 3 reports Provet's improvements relative to other architectures for each tested configuration. These improvements are calculated as the ratio between Provet's average utilization and the best utilization achieved by the other architectures, with the same procedure used to determine the compute-to-memory ratio.

All the discussed architectures, including the proposed one, are capable of attaining considerable levels of utilization during the execution of conventional convolution operations in popular neural networks like AlexNet and ResNet. However, it can be observed that SAs utilization can dip below 75% when it comes to larger kernels.

This drop in utilization can be attributed to two main factors: the rigid interconnect and the size mismatches. Refer to section 3.2 for a more detailed explanation.

Table 3. Improvement of Provet over other architectures for ResNet (RN), AlexNet (AN) and MobileNet (MN) convolution layers for different kernel sizes. **Red values are preliminary estimations**

Layer	Utilization improvement				CMR improvement			
	Eyeriss	TPU	ARA	GPU	Eyeriss	TPU	ARA	GPU
RN_112x112	x1.70	x1.08	x1.01	x15.97	x4.09	x3.00	x1.36	x1.25
RN_56x56	x1.37	x1.03	x1.04	x9.71	x3.63	x3.00	x1.24	x1.21
RN_28x28	x1.03	x0.98	x1.11	x15.42	x4.14	x3.03	x1.28	x1.11
RN_14x14	x1.19	x1.10	x1.20	x19.12	x4.00	x3.29	x1.31	x1.26
RN_7x7	x1.18	x2.50	x1.18	x17.67	x3.60	x3.33	x1.53	x1.61
AN_55x55	x1.32	x1.06	x1.01	x13.04	x3.95	x3.48	x1.50	x1.16
AN_27x27	x1.05	x1.31	x1.12	x15.65	x4.24	x3.07	x1.41	x1.20
AN_13x13	x0.94	x1.09	x1.05	x16.05	x4.09	x3.00	x1.48	x1.00
MN_112x112	x3.18	x2.00	x1.08	x12.15	x25.00	x15.00	x3.13	x2.14
MN_56x56	x5.00	x3.75	x1.06	x8.05	x19.50	x15.60	x2.69	x3.00
MN_7x7	x9.43	x3.67	x1.10	x5.04	x24.67	x18.50	x2.96	x3.08

A more significant difference in utilization can be observed in the MobileNet layers which exhibits a less regular data-flow pattern with less exploitable data reuse thus imposing greater demands on memory bandwidth. When the memory bandwidth is not sufficient to keep all PEs the utilization degrades. This situation can be observed for all MobileNet layers in Figure 9. Eyeriss and TPU utilization collapse to very low numbers due to a severe memory bottleneck. However, Provet and ARA can maintain reasonable utilization numbers thanks to the much higher memory bandwidth available.

In addition to the PE utilization shown in Figure 9, the compute-to-memory access ratio was also evaluated for the same mappings. These findings are presented in Figure 10. Notably, Provet exhibits a significantly higher compute-to-memory ratio, indicating that more computations are performed for each global memory access compared to Eyeriss, TPU, and ARA.

This distinction is especially pronounced for MobileNet mappings, where the level of data reuse is substantially lower than that in ResNet or AlexNet. As described in section ??, SAs depend on data reuse as the primary method to minimize memory access, thereby maximizing the compute-memory ratio. However, Provet utilizes the memory asymmetry of the VWR to minimize memory access operations. Although Provet also benefits from local data reuse, its architectural differences allow for a better compute-to-memory ratio even under conditions of reduced data reuse.

The overall findings match the expectations derived from the theoretical analysis of the architectures presented in the earlier sections. The mixture of a 1D organization, the intermediate memory (VWR) and the data shufflers, allow Provet to achieve higher utilization and better compute-to-memory ratios than the other architectures.

In addition to the utilization and compute-to-memory ratio, which are the primary metrics for evaluating the improvements of Provet innovations, we have also considered the memory accesses and latency for the same convolutional kernels. These metrics are presented in Table 4 and summarized in Figure 11a. The memory accesses are calculated as the number of reads from the global memory, as defined in 1. The latency is calculated as the time to process an individual layer, including the time to read the input data, perform the computations, and write the results back.

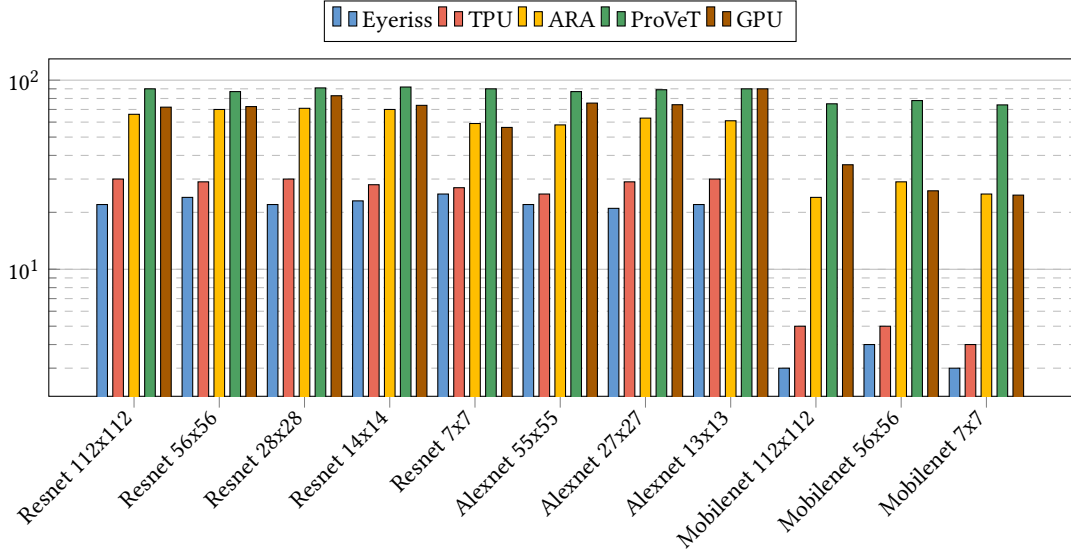


Fig. 10. Compute-to-memory access ratio for different layers of state-of-the-art CNNs.

Table 4. Memory accesses and latency for different architectures. All values are scaled [22] to an equivalent 28 nm technology node and 200 MHz clock frequency.

Layer	MOPS	Eyeriss		TPU		ARA		A100		Provet	
		Reads	Latency	Reads	Latency	Reads	Latency	Reads	Latency	Reads	Latency
Resnet 112x112	236.0	22.434	9.231	33.891	0.320	15.125	5.657	90.287	1.757	6.611	0.193
Resnet 56x56	231.2	22.093	9.035	33.058	0.315	14.820	5.516	88.416	1.713	6.454	0.189
Resnet 28x28	115.6	11.025	4.492	16.587	0.156	7.398	2.777	44.302	0.856	3.223	0.095
Resnet 14x14	115.6	11.072	4.536	16.493	0.157	7.414	2.785	44.258	0.861	3.222	0.095
Resnet 7x7	115.6	11.067	4.551	16.609	0.157	7.344	2.752	44.230	0.859	3.189	0.095
Alexnet 55x55	210.8	20.156	8.257	30.189	0.286	13.456	5.029	80.055	1.550	5.834	0.171
Alexnet 27x27	895.8	85.803	34.885	127.607	1.223	57.337	21.333	342.714	6.639	24.942	0.729
Alexnet 13x13	299.0	28.512	11.630	42.560	0.406	19.174	7.107	114.604	2.211	8.363	0.244
Mobilenet 112x112	0.7	0.131	1.125	0.191	0.435	0.088	0.954	0.512	3.059	0.038	0.339
Mobilenet 56x56	1.8	0.340	0.768	0.515	0.510	0.231	1.071	1.374	3.651	0.101	0.403
Mobilenet 7x7	0.5	0.090	0.689	0.131	0.218	0.057	0.887	0.343	2.089	0.025	0.230

The results show a significant reduction in global memory accesses for Proved when compared to other architectures, more notably for systolic arrays and GPUs as anticipated. The latency<sup>1</sup> is also significantly lower for Provet, which is a direct consequence of the high utilization achieved in its processing elements. An important observation is that vector processors (Provet and ARA) have the lowest total amount of memory accesses, which confirms the motivations presented in section 3. Finally, GPUs provide a very low latency, but fail to achieve low memory accesses when batch size is set to 1, as its ability to exploit data reuse is severely hindered. Other architectures on the other hand, can exploit some level of data reuse even when the batch size is set to 1.

<sup>1</sup>Latency results are scaled to a 200 MHz clock and equivalent 28 nm technology node.

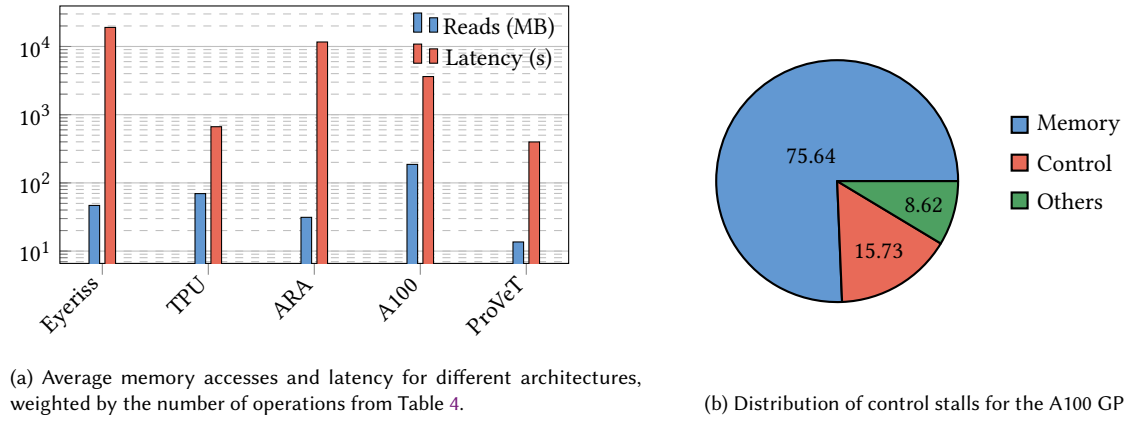


Fig. 11

## 8 CONCLUSIONS

This paper has proposed an innovative memory hierarchy that effectively addresses the challenge of memory bandwidth in data-parallel AI/ML applications. By introducing three levels of on-chip memory hierarchy - local, intermediate, and global - with ultra-wide registers and specialized data-shufflers, the proposed architecture improves versatility and adaptivity to varying data-parallel applications, even for those with limited data reuse. The mapping of a representative data parallel application, such as a convolutional neural network, to the proposed architecture highlights its superiority over existing systolic array-based ML/AI architectures in terms of memory bandwidth bottlenecks. We demonstrate how a set of mappings can be used to construct a library that enables developers to quickly and easily map their application onto the proposed wide-shallow memory hierarchy. By leveraging this library, developers can accelerate the development process and focus on optimizing their applications for performance and power rather than spending significant time on memory hierarchy design. This approach not only simplifies the design process, but also enables the development of highly efficient AI/ML applications that take full advantage of the proposed memory hierarchy. Additionally, our study showed that scaling a wide-shallow memory is a better approach than using a square memory design.

## ACKNOWLEDGEMENTS

This work has been supported by IMEC, Leuven, Belgium.

## REFERENCES

- [1] John Backus. 2007. *Can programming be liberated from the von Neumann style? a functional style and its algebra of programs*. Association for Computing Machinery, New York, NY, USA, 1977. <https://doi.org/10.1145/1283920.1283933>
- [2] Amirali Boroumand, Saugata Ghose, Berkin Akin, Ravi Narayanaswami, Geraldo F Oliveira, Xiaoyu Ma, Eric Shiu, and Onur Mutlu. 2021. Google neural network models for edge devices: Analyzing and mitigating machine learning inference bottlenecks. In *2021 30th International Conference on Parallel Architectures and Compilation Techniques (PACT)*. IEEE, 159–172.
- [3] Amirali Boroumand, Saugata Ghose, Berkin Akin, Ravi Narayanaswami, Geraldo F Oliveira, Xiaoyu Ma, Eric Shiu, and Onur Mutlu. 2021. Mitigating edge machine learning inference bottlenecks: An empirical study on accelerating Google edge models. *arXiv preprint arXiv:2103.00768* (2021).
- [4] Amirali Boroumand, Saugata Ghose, Youngsok Kim, Rachata Ausavarungrun, Eric Shiu, Rahul Thakur, Daehyun Kim, Aki Kuusela, Allan Knies, Parthasarathy Ranganathan, and Onur Mutlu. 2018. Google Workloads for Consumer Devices: Mitigating Data Movement Bottlenecks. In *Proceedings of the Twenty-Third International Conference on Architectural Support for Programming Languages and Operating Systems* (Williamsburg, VA, USA)

- (ASPLOS '18). Association for Computing Machinery, New York, NY, USA, 316–331. doi:10.1145/3173162.3173177
- [5] Tianshi Chen, Zidong Du, Ninghui Sun, Jia Wang, Chengyong Wu, Yunji Chen, and Olivier Temam. 2014. Diannao: A small-footprint high-throughput accelerator for ubiquitous machine-learning. *ACM SIGARCH Computer Architecture News* 42, 1 (2014), 269–284.
  - [6] Yu-Hsin Chen, Joel Emer, and Vivienne Sze. 2016. Eyeriss: A Spatial Architecture for Energy-Efficient Dataflow for Convolutional Neural Networks. *SIGARCH Comput. Archit. News* 44, 3 (jun 2016), 367–379. doi:10.1145/3007787.3001177
  - [7] Yu-Hsin Chen, Joel Emer, and Vivienne Sze. 2016. Eyeriss: A Spatial Architecture for Energy-Efficient Dataflow for Convolutional Neural Networks. In *Proceedings of the 43rd International Symposium on Computer Architecture* (Seoul, Republic of Korea) (ISCA '16). IEEE Press, 367–379. doi:10.1109/ISCA.2016.40
  - [8] NVIDIA Corporation. 2023. *NVIDIA CUDA Basic Linear Algebra Subroutines (cuBLAS) Library*. NVIDIA Corporation. Version 11.x or higher.
  - [9] Vidushi Dadu, Jian Weng, Sihao Liu, and Tony Nowatzki. 2019. Towards General Purpose Acceleration by Exploiting Common Data-Dependence Forms. In *Proceedings of the 52nd Annual IEEE/ACM International Symposium on Microarchitecture* (Columbus, OH, USA) (MICRO '52). Association for Computing Machinery, New York, NY, USA, 924–939. doi:10.1145/3352460.3358276
  - [10] Paul Delestrac, Debjyoti Battacharjee, Simei Yang, Diksha Moolchandani, Francky Catthoor, Lionel Torres, and David Novo. 2024. Multi-level Analysis of GPU Utilization in ML Training Workloads. In *2024 Design, Automation & Test in Europe Conference & Exhibition (DATE)*. IEEE, 1–6.
  - [11] Paul Delestrac, Jonathan Miquel, Debjyoti Bhattacharjee, Diksha Moolchandani, Francky Catthoor, Lionel Torres, and David Novo. 2024. Analyzing GPU Energy Consumption in Data Movement and Storage. In *Proceedings of the 35th IEEE Conference on Application-specific Systems, Architectures and Processors (ASAP)*.
  - [12] John A. Gunnels, Greg M. Henry, and Robert A. van de Geijn. 2001. A Family of High-Performance Matrix Multiplication Algorithms. In *Computational Science — ICCS 2001*, Vassil N. Alexandrov, Jack J. Dongarra, Benjie A. Juliano, René S. Renner, and C. J. Kenneth Tan (Eds.). Springer Berlin Heidelberg, Berlin, Heidelberg, 51–60.
  - [13] Andrew G. Howard, Menglong Zhu, Bo Chen, Dmitry Kalenichenko, Weijun Wang, Tobias Weyand, Marco Andreetto, and Hartwig Adam. 2017. MobileNets: Efficient Convolutional Neural Networks for Mobile Vision Applications. *CoRR* abs/1704.04861 (2017). arXiv:1704.04861 <http://arxiv.org/abs/1704.04861>
  - [14] Norman P. Jouppi, Andrew B. Kahng, Naveen Muralimanohar, and Vaishnav Srinivas. 2012. CACTI-IO: CACTI with off-chip power-area-timing models. In *2012 IEEE/ACM International Conference on Computer-Aided Design (ICCAD)*. 294–301.
  - [15] Norman P. Jouppi, Cliff Young, Nishant Patil, David Patterson, Gaurav Agrawal, Raminder Bajwa, Sarah Bates, Suresh Bhatia, Nan Boden, Al Borchers, Rick Boyle, Pierre-luc Cantin, Clifford Chao, Chris Clark, Jeremy Coriell, Mike Daley, Matt Dau, Jeffrey Dean, Ben Gelb, Tara Vazir Ghaemmaghami, Rajendra Gottipati, William Gulland, Robert Hagmann, C. Richard Ho, Doug Hogberg, John Hu, Robert Hundt, Dan Hurt, Julian Ibarz, Aaron Jaffey, Alek Jaworski, Alexander Kaplan, Harshit Khaitan, Daniel Killebrew, Andy Koch, Naveen Kumar, Steve Lacy, James Laudon, James Law, Diemthu Le, Chris Leary, Zhuyuan Liu, Kyle Lucke, Alan Lundin, Gordon MacKean, Adriana Maggiore, Maire Mahony, Kieran Miller, Rahul Nagarajan, Ravi Narayanaswami, Ray Ni, Kathy Nix, Thomas Norrie, Mark Omernick, Narayana Penukonda, Andy Phelps, Jonathan Ross, Matt Ross, Amir Salek, Emad Samadiani, Chris Severn, Gregory Sizikov, Matthew Snelham, Jed Souter, Dan Steinberg, Andy Swing, Mercedes Tan, Gregory Thorson, Bo Tian, Horia Toma, Erick Tuttle, Vijay Vasudevan, Richard Walter, Walter Wang, Eric Wilcox, and Doe Hyun Yoon. 2017. In-Datacenter Performance Analysis of a Tensor Processing Unit. In *Proceedings of the 44th Annual International Symposium on Computer Architecture* (Toronto, ON, Canada) (ISCA '17). Association for Computing Machinery, New York, NY, USA, 1–12. doi:10.1145/3079856.3080246
  - [16] Svilen Kanev, Juan Pablo Darago, Kim Hazelwood, Parthasarathy Ranganathan, Tipp Moseley, Gu-Yeon Wei, and David Brooks. 2015. Profiling a warehouse-scale computer. In *Proceedings of the 42nd annual international symposium on computer architecture*. 158–169.
  - [17] Youngeun Kwon and Minsoo Rhu. 2018. Beyond the memory wall: A case for memory-centric hpc system for deep learning. In *2018 51st Annual IEEE/ACM International Symposium on Microarchitecture (MICRO)*. IEEE, 148–161.
  - [18] Linyan Mei, Pouya Houshmand, Vikram Jain, Sebastian Giraldo, and Marian Verhelst. 2021. ZigZag: Enlarging Joint Architecture-Mapping Design Space Exploration for DNN Accelerators. *IEEE Trans. Comput.* 70, 8 (2021), 1160–1174. doi:10.1109/TC.2021.3059962
  - [19] NVIDIA Corporation. March 2020. *White paper: NVIDIA AMPERE GA102 GPU architecture*. Technical Report. <https://www.nvidia.com/content/PDF/nvidia-ampere-ga-102-gpu-architecture-whitepaper-v2.pdf>
  - [20] Angshuman Parashar, Priyanka Raina, Yakun Sophia Shao, Yu-Hsin Chen, Victor A. Ying, Anurag Mukkara, Rangharajan Venkatesan, Brucek Khailany, Stephen W. Keckler, and Joel Emer. 2019. Timeloop: A Systematic Approach to DNN Accelerator Evaluation. In *2019 IEEE International Symposium on Performance Analysis of Systems and Software (ISPASS)*. 304–315. doi:10.1109/ISPASS.2019.00042
  - [21] Matteo Perotti, Matheus Cavalcante, Nils Wistoff, Renzo Andri, Lukas Cavigelli, and Luca Benini. 2022. A “New Ara” for Vector Computing: An Open Source Highly Efficient RISC-V V 1.0 Vector Processor Design. In *2022 IEEE 33rd International Conference on Application-specific Systems, Architectures and Processors (ASAP)*. 43–51. doi:10.1109/ASAP54787.2022.00017
  - [22] Satyabrata Sarangi and Bevan Baas. 2021. DeepScaleTool: A Tool for the Accurate Estimation of Technology Scaling in the Deep-Submicron Era. In *2021 IEEE International Symposium on Circuits and Systems (ISCAS)*. 1–5. doi:10.1109/ISCAS51556.2021.9401196
  - [23] Pablo Villalobos, Jaime Sevilla, Lennart Heim, Tamay Besiroglu, Marius Hobbhahn, and Anson Ho. 2022. Will we run out of data? an analysis of the limits of scaling datasets in machine learning. *arXiv preprint arXiv:2211.04325* 1 (2022).
  - [24] Shimeng Yu, Hongwu Jiang, Shanshi Huang, Xiaochen Peng, and Anni Lu. 2021. Compute-in-memory chips for deep learning: Recent trends and prospects. *IEEE circuits and systems magazine* 21, 3 (2021), 31–56.

- [25] Jiyuan Zhang, Franz Franchetti, and Tze Meng Low. 2018. High Performance Zero-Memory Overhead Direct Convolutions. arXiv:1809.10170 [cs.LG] <https://arxiv.org/abs/1809.10170>
- [26] Yangjie Zhou, Mengtian Yang, Cong Guo, Jingwen Leng, Yun Liang, Quan Chen, Minyi Guo, and Yuhao Zhu. 2021. Characterizing and Demystifying the Implicit Convolution Algorithm on Commercial Matrix-Multiplication Accelerators. In *2021 IEEE International Symposium on Workload Characterization (IISWC)*. 214–225. doi:10.1109/IISWC53511.2021.00029